TRMM Final Report for the first three years of
NASA Grant NAG5-1586

TRMM-Related Research
Tropical Rainfall and Energy Analysis Experiment

Principle Investigator: Verner E. Suomi
Co-Investigators: S. Ackerman, B. Hinton and D. Martin

May 1994

INTRODUCTION

The overall science objective of our participation in TRMM is the determination of daily rainfall and latent heating in the tropical atmosphere using TRMM and complementary spacecraft observations. Our major focus these first three years has been to extend, in space and time, the TRMM satellite observations of rainfall. Observations from TRMM active and passive microwave radiometers will provide the fundamental observations for understanding the hydrological cycle of the tropics. Due to the orbit of the TRMM satellite and the extreme variability of convective rain systems, the TRMM observations provide rainfall estimates representative of a one month period. Monthly mean rainfall rates provide valuable information; however, in our view, this time scale limitation neglects the great value of the data towards a better understanding of the physics of tropical convection. Many tropical periodicities will not be characterized by these monthly averages, e.g. diurnal cycles, the 4-6 day easterly waves and the 30-60 day cycle. In the spatial domain, due to its orbit, the TRMM satellite will over-fly many convective systems only once. Indeed, some precipitating systems will not be sampled at all.

Observations from geostationary satellites can be used to extend the TRMM observations to smaller time and space scales. Although geostationary satellites cannot probe the interiors of precipitating systems, they do observe their life-cycles. To acquire information on cloud water content and rain rate, we propose to combine geostationary and other satellite observations with the TRMM satellite measurements. In these pre-mission years, we will use DMSP microwave, TOGA radar and other observations as proxies for TRMM.

WORK COMPLETED UNDER THIS PROPOSAL

Cloud Classification Scheme

Cloud classification methods have been developed using bi- or tri-spectral methods for data from the GOES, GMS and Meteosat satellites. Pattern recognition is another important method for characterizing cloud type and coverage. These techniques are more demanding than pixel based methods but provide more information. Our approach for specifying the rain classes is to analyze pattern and texture in multi-spectral images from geostationary satellites. Our present classification scheme is rooted in the algorithm developed by Garand (1988) for the north Atlantic. The method uses visible (VIS) and infrared (IR) images from a geostationary satellite to classify cloud in a 128×128 km region, or classification box. Garand's twenty cloud classes are illustrated in Figure 1. For each cloud class there are four examples. Each example consists of two parts: a view in VIS (above) and a view in IR (below). White numerals are the cloud class numbers.

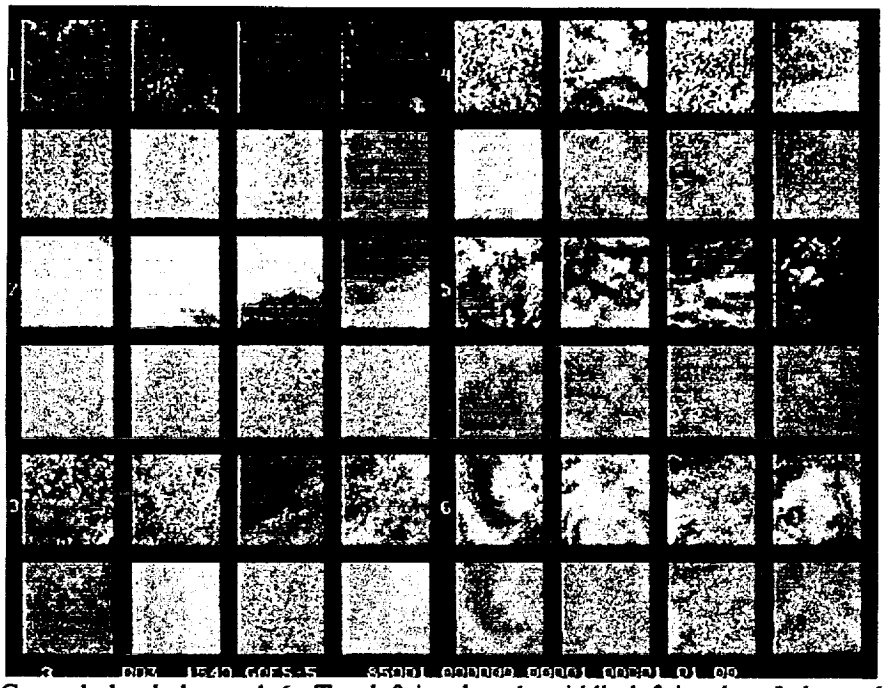

Figure 1. Garand cloud classes 1-6. Top-left is class 1, middle-left is class 2, lower-left is class 3, top-right is class 4, middle-right is class 5 and lower-right is class 6. Continued.

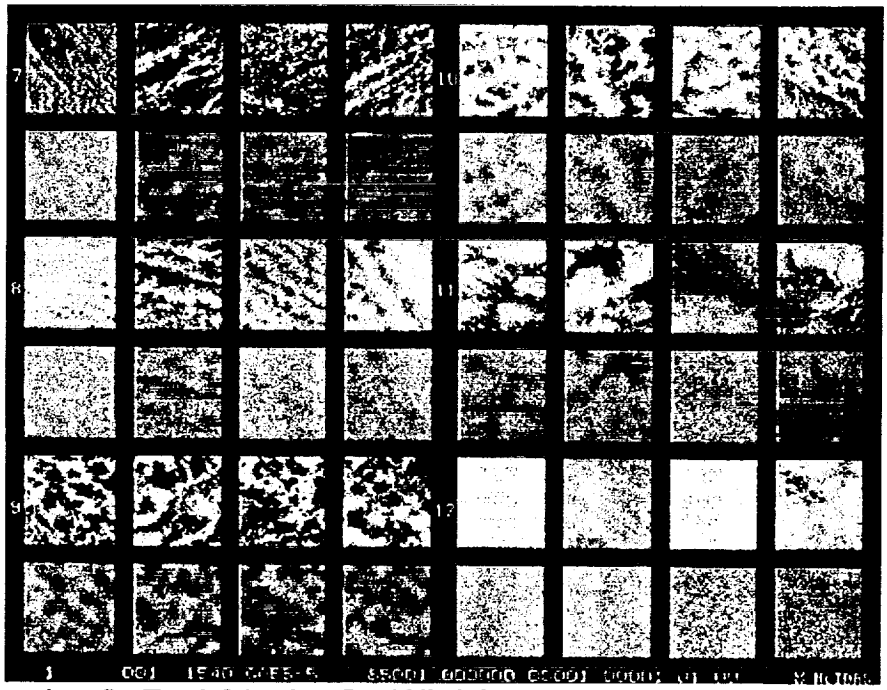

Figure 1 (continued). Top-left is class 7, middle-left is class 8, lower-left is class 9, top-right is class 10, middle-right is class 11 and lower-right is class 12. Continued.

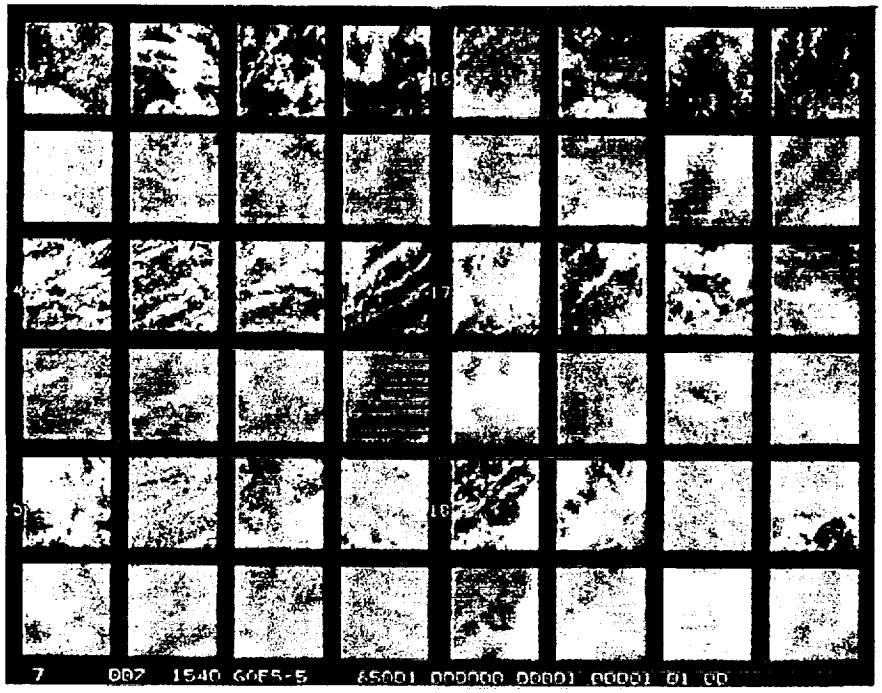

Figure 1 (continued). Top-left is Class 13, middle-left is class 14, lower-left is class 15, upper-right is class 16, middle-right is class 17 and lower-right is class 18. Continued.

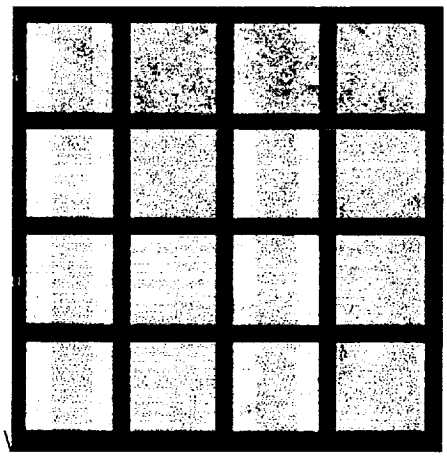

Figure 1 (concluded). Top is class 19 and bottom is class 20.

We have enhanced the original algorithm to include the following options:

1. The VIS and IR observations both can have a nominal spatial resolution of 4 km at nadir rather than 1 km data sampled at 2 km intervals. This change will allow us to process GMS (approximately 4 km) and Meteosat (approximately 5 km) observations in a consistent global analysis.
2. To set the clear sky IR temperature threshold, NMC sea surface temperature (SST) data rather than climatological SST data is imported into the algorithm. Presently the threshold for cloud is $T_{11} \leq (SST-4°)$. This change should result in an improved rain classification.
3. To extend coverage to nighttime hours the algorithm can be run with IR data alone.
4. The algorithm is being adapted to the tropical oceans. This entails verification by comparison with subjectively determined parameters as well as verification by comparison with parameters retrieved from satellite microwave observations..
5. Anisotropic factors have been included for determining clear sky thresholds for the tropical oceans. This change also entails subjective verification.

Using GOES images of the eastern tropical Pacific, we tested the performance of the modified cloud classification scheme and its utility in estimating rain. In the eastern Pacific there are neither independent classifications of cloud nor independent measurements of rain. Lacking independent observations, Garand trained the algorithm on subjective estimates of cloud type. To verify the McIDAS cloud classes, we followed the methodology of Garand (1988), except that the analyst could view up to three image pairs rather than the "target" image pair only. (One of the supplemental image pairs was a half hour older than the target image pair; the second was a half hour younger.) Looping the triplet enabled the analyst (D. Martin) to resolve some ambiguous situations through differential movement of clouds. Martin was one of two analysts who assisted Garand in the validation of the original algorithm.

For classification boxes in a subset of images Martin also estimated rain class. Classes consist of nil, light, moderate and heavy (S0, S1, S2 and S3). Nominal rates are <0.05, 0.05 to 1.0, 1.0 to 10 and >10 mm/h, respectively. Rain classes were assigned on the basis of bispectral radiance, texture, pattern and behavior (see Martin and Howland 1986); never on the basis of the McIDAS cloud class.

We found, as expected, that there is a clear association of cloud class with rain class. This is evident in Figure 2. Part (a) shows the frequency of cloud class as a function of rain class. The nil-rain class contains many boxes; the heavy-rain class contains few boxes. Within the "nil" rain class boxes fall mainly in the "clear" cloud class (1); some fall also in classes of scattered-shallow-cumulus-cells, altocumulus-clouds and thin-cirrus (3, 13 and 16, respectively). Within the "moderate" and "heavy" rain classes boxes tend to cluster in the "multi-layer-cirrus" and "thick-cirrus" cloud classes (18 and 19). Part (b) of Figure 2 replots the information in part (a) as percentage occurrence of rain classes given some cloud class. Of the 38 boxes which the algorithm classified as "scattered shallow cumulus cells", the analyst classified 35 (92 %) as "nil" rain and the remaining 3 (7 %) as "light" rain. Of the five boxes which the algorithm classified as "overcast thick cirrus", the analyst classified one as "light" rain, one as "moderate" rain and three as "heavy" rain.

Up to one-fifth of the Garand's original classes may not be relevant to cloud classification in the equatorial tropics. This is suggested by Figure 3, which shows the frequency of occurrence of cloud classes for the rain sectors. The sample consists of 239 boxes. Of the classes representing species of cumulus (3, 4, 7, 8, 9,10 and 11) only two were assigned. The algorithm did not classify any boxes as nimbostratus (class 12) or as cumulonimbus (class 20). The evident presence of these species argues for tuning the classification coefficients to the tropics. (Following this study, a revised calibration of the GOES visible channel was included in the algorithm. Cloud albedo plays a prominent role in assigning a cumulonimbus classification and the revised calibration allows for regions to be assigned this class.)

Especially in the context of rain estimation, it suggests that additional classes may be needed; for example, a "popcorn" cumulonimbus class.

It is clear that while McIDAS "Garand" algorithms can indeed classify rain cloud types, the addition of parameters will improve estimates. Tests to do this are an important part of our future research.

a)

b)

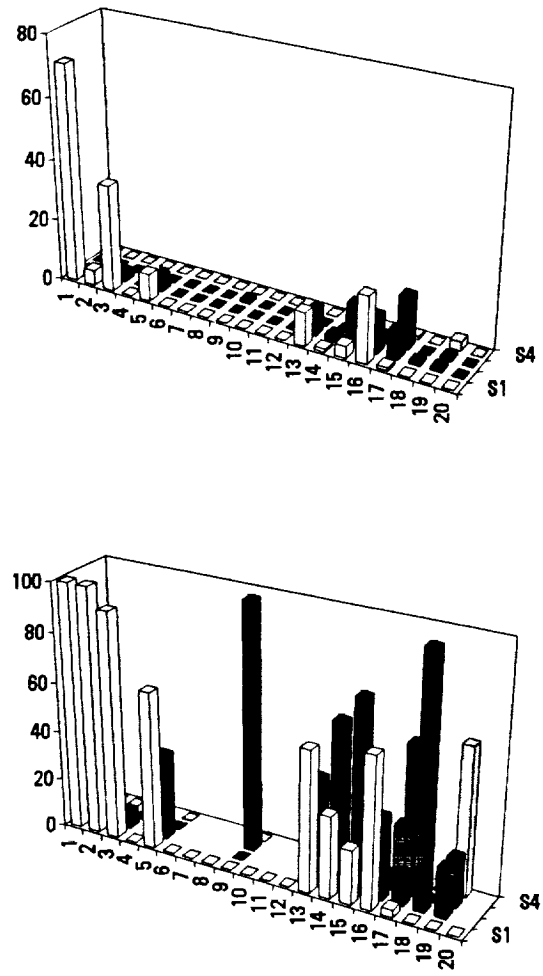

Figure 2. Cloud class vs. rain class. Part (a) is a 3-D histogram. Part (b) is a 3-D probability distribution, expressed in percent and conditioned on the occurrence of some cloud class. If a cloud class occurs, the probabilities at the rain classes totals 100 %.

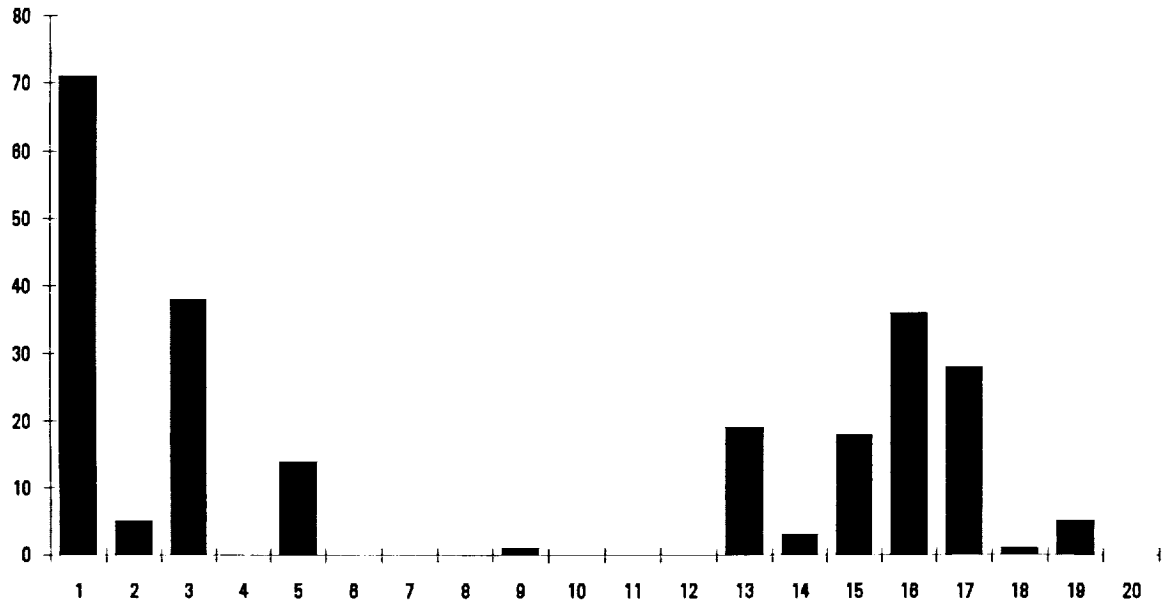

Figure 3. Histogram of cloud classes for the rain test. Class 1 is clear. Classes 2-15 are water clouds; classes 16-20 are ice or ice/water clouds. Within the water group classes 2-12 are low clouds and classes 13-15 are middle-clouds.

Relation of GMS IR to Rainfall Established with Microwave Radiance

To estimate tropical rainfall the Global Precipitation Climatology Project employs a thermal infrared method, the GOES Precipitation Index. Operating on a scale that includes many clouds, GPI selects "rain fraction" using a 235 K threshold applied to images in the 11 μm window channel of geostationary spacecraft. This rain fraction is assigned a rain rate of $3\ mm\ h^{-1}$. On a cloud system scale it has been speculated (e.g. see Adler *et al.* 1993, Kummerow and Giglio 1992 and Vicente and Anderson 1993) that passive microwave observations could be used to tune the threshold or the rate to a region or a time. On an individual cloud scale the increased latent heating associated with more intense rain might increase the raining parcel's buoyancy tending to produce cloud at higher levels and (since at reduced pressure the parcel expands) cooler temperatures. This relationship suggests a scheme in which rain rate is variable, increasing as the cloud top temperature decreases below a threshold (e.g. see Goodman *et al.* 1993). To test these ideas we analyzed Geostationary Meteorological Satellite (GMS) and SSMI data from TOGA/COARE.

The relationship between rain rate and cloud top temperature is modulated by several factors, including, for example, the profile of temperature and the degree of entrainment of non-precipitating environmental air. In addition, shear can produce a parallax between the coldest part of the cloud tower and the precipitation. Equally important are non-precipitating cloud particles, especially cirrus, which can persist after the precipitation associated with their formation has fallen.

Thus any collection of observations consisting of IR and simultaneous observations of rain rate will exhibit a distribution of rain rates for a given IR brightness temperature. The best we can hope for is that the mean relation will be stable and the standard deviation will be small enough to make the estimate useful. Additional information about the cloud might refine the mean relation and narrow the dispersion. For example, if a high cloud is detached cirrus, rather than the top of a cumulonimbus, its assigned rain rate would be lower.

Since in our TOGA/COARE investigation the IR and microwave data are not from the same platforms, it was necessary to tolerate small time differences (±0.25 hours). It also was necessary to remap one satellite's view into the other, which cannot be done without some perspective distortion.

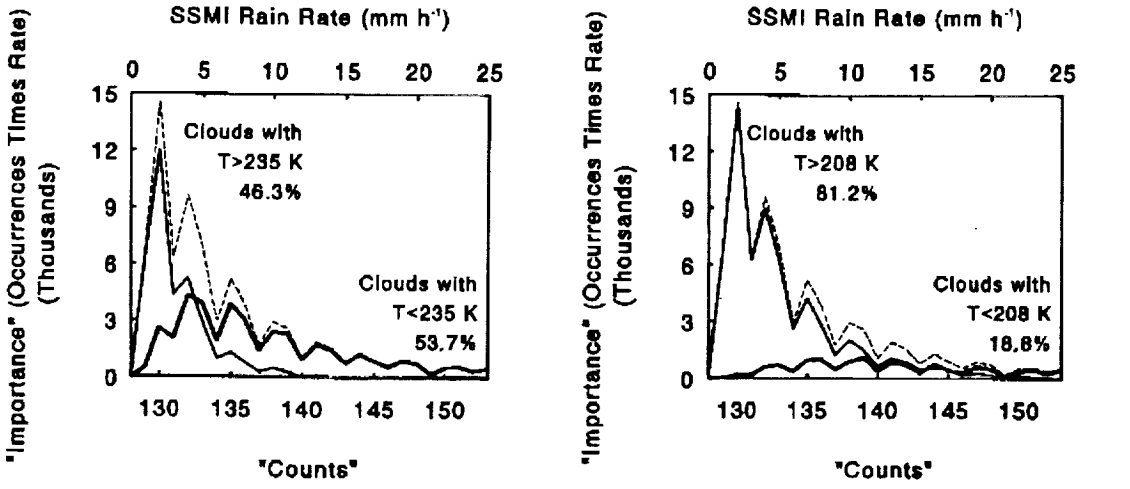

Figure 4. Effect of varying the brightness temperature threshold on rain rates associated with clouds at or colder than the threshold. Rain rate is the upper *x*-axis (lower axis is an arbitrary unit). The "importance" plotted on the *y*-axis is the number of occurrences (n) of a given rain rate (R) times the rain rate [*i.e.*, $n(R) \bullet R$].

Figure 4 illustrates the effect of changing the black body temperature threshold. In both panels the dotted curve shows the rain rate distribution for *all* clouds, both above and below the indicated threshold (*i.e.* 235, at left, or 208 K, at right). Rain rate is indicated on the upper x-axis. The medium-weight solid line illustrates the rain rate distribution for clouds *warmer* than the threshold, while the bold line shows the distribution for clouds *colder* than the threshold. Note that the peak of the colder cloud curve always lies to the right of the peak of the warmer cloud curve. Note also that only the colder than 208 K curve has a long tail on the low-rate side of the peak. These and other results of the study suggest that a temperature-dependent rain rate would be superior to a fixed rain rate.

Integration of GOES and DMSP SSMI data

We have fully integrated SSMI data from the DMSP satellite with the GOES observations. Incorporation of the SSMI measurements provides independent information on total precipitable water (PW), cloud liquid water content (LWC) and rain rate (RR). If they are within 10 minutes of a GOES image, which is available every half hour, the SSMI data are remapped into the GOES projection. As with TRMM, we only consider tropical regions. An example of the re-mapping is given in the Figure 5. In this figure, the GOES infrared channel image is depicted in black and white, overlain with a a color image of the remapped the SSMI derived cloud liquid water content. As would be expected, the liquid water content is large (red values) for the 'hot towers'. Note also that the SSMI does not sample the entire cloud system.

Individual SSMI values are composited for each classification box. While all the SSMI spectral observations are available to the classification algorithm, we use the derived products only. The average PW is derived by averaging all values within a box. The average SSMI LWC and RR for each box are computed in two ways: 1) averaging only non-zero values and 2) including zero values in the mean. Standard deviations for each value are also computed for each box.

In addition to the SSMI observations the classification scheme also incorporates GOES radiances at 12 μm and 6.7 μm. Nominal resolutions of these infrared channels at nadir are 8 km and 16 km,

respectively. Because neither channel adds pattern information, we do not compute class discrimination features such as the two-dimensional power spectrum for the boxes. Instead, for each quadrant mean, maximum, minimum, and standard deviation brightness temperatures are computed.

The 12 μm channel is used in conjunction with the 11 μm channel as a GOES version of Inoue's (1987) split window rain discriminator. He has observed, as we have, negative brightness temperature differences (11 μm minus 12 μm) which are correlated with convective cells. Figure 6 is a set of histograms of SSMI derived rain rates averaged over the boxes. Boxes are stratified by the brightness temperature difference between 11 and 12 microns (BT_{11}-BT_{12}). The upper two panels show rain rate frequency for BT_{11}-$BT_{12} \leq 0$ (left) and BT_{11}-$BT_{12} \leq -1$ (right). The lower panels show rain rate frequency for positive brightness temperature differences. Note that the heavy rain rates generally occur for negative values, though it is possible to have no rain and still have negative brightness temperature differences.

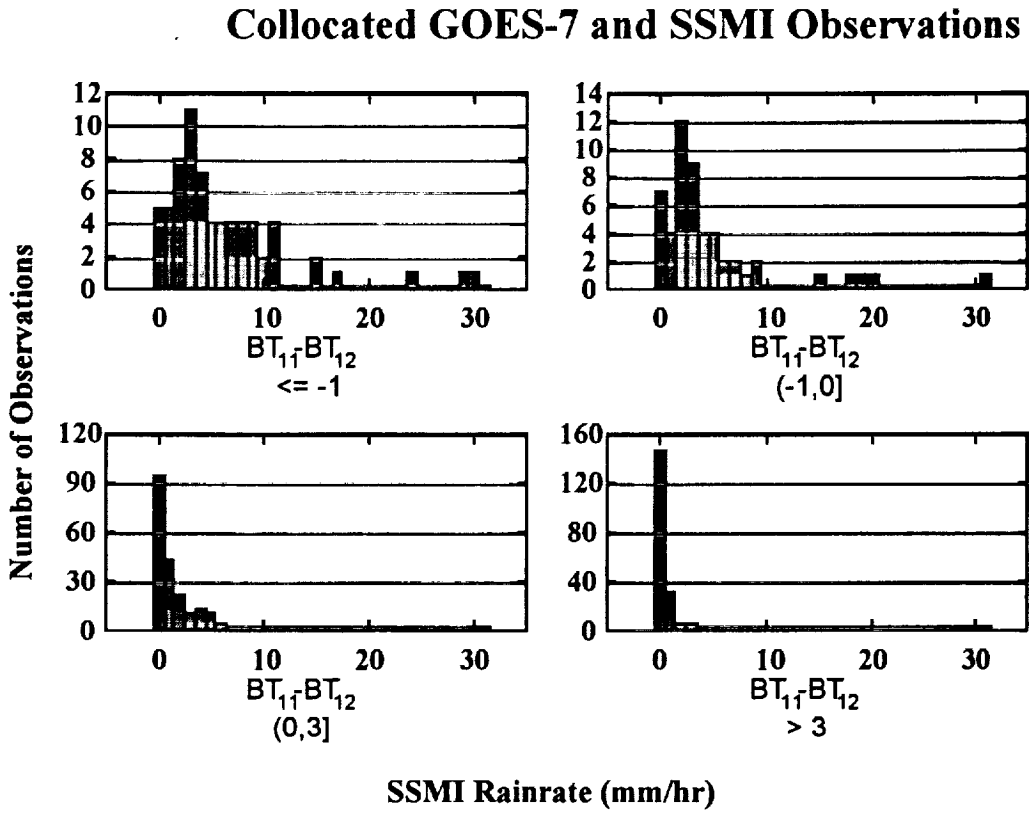

Figure 6. Histogram of SSMI rain rate categorized by the brightness temperature difference between observations at 11 and 12 μm. The categories are listed below each of the four panels.

Detecting Convective Cores using 11 and 6.7 micron observations

The 6.7 μm spectral channel is sensitive to the relative humidity averaged over an atmospheric depth extending from approximately 200 to 500 mb, and is very sensitive the presence of cirrus. Figure 7 is a histogram of the SSMI rain rates stratified by the difference between the 11 μm and the 6.7 μm equivalent temperatures. Whenever the brightness temperature difference is less than zero (left panel), the SSMI indicates rain. This is potentially much more valuable than the split window difference. If it is reliable, this brightness temperature difference would be extremely valuable predictor in characterizing a precipitation system.

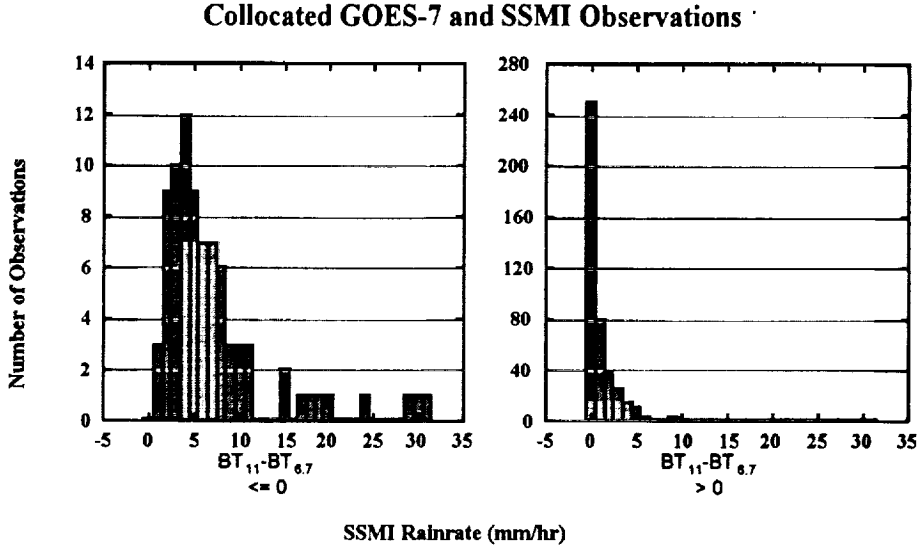

Figure 7. Histogram of SSMI rain rate categorized by the brightness temperature difference between observations at 11 and 6.7 μm. The categories are listed below each of the two panels

Figure 8 depicts the geographic location of each occurrence of a negative difference during July 1993 and January 1994. This Figure was generated from the NOAA-12 polar orbiting satellite using the High-resolution Infrared Sounder (HIRS/2) 11 and 6.7 μm spectral observations. Each circle represents the geographical location of a single HIRS/2 field-of-view (FOV) within 40 north and south latitude which displayed the negative difference in BT_{11}-$BT_{6.7}$. The differences correlate highly with expected regions of convection. The Intertropical Convergence Zone (ITCZ) is apparent in both months, as is the shift in its position to the summer hemisphere. The summertime peak in convection over South America and convection associated with the southwest summer monsoon are also clearly visible. Regions with no monthly deep convective systems also manifest themselves in this composite analysis. In addition to regions favorable to tropical convection, negative differences also appear in the mid-latitude storm tracks of the winter hemisphere. These negative values (which appear to be associated with the convective core) are an extremely useful tool for studying the hydrological cycle. Convective activity is extremely variable in both time and space, as is evident by plotting the geographic location of the negative differences for a single day (Figure 9). On any given day only a very small portion of the globe is convectively active - as indicated by these observations. The 11 and 6.7 μm observations are currently available on the GOES and METEOSAT geostationary satellites and the NOAA polar orbiting satellites providing the spatial completeness and temporal continuity required for studying tropical convection. The capability to locate the convective core has an important impact on TRMM activities.

JULY 1993

JANUARY 1994

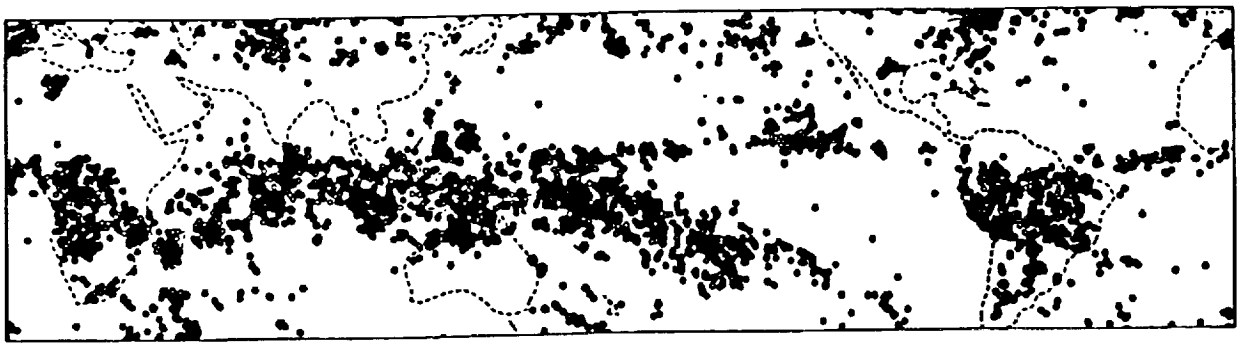

Figure 8. Location of negative BT_{11}-$BT_{6.7}$ as observed by the NOAA-12 HIRS/2 instrument for the months of July 1993 and January 1994. Each circle represents the geographic location of an occurrence.

JANUARY 12, 1994

Figure 9. Same as Figure 8 except observations are for a single day.

Participation in TRMM Science Team Meetings

Last but not least, the principle investigator was an active participate in the Mission Facility Team's deliberations to insure the maximum science return from the mission.

RELATED PUBLICATIONS

Martin, D. W., B. B. Hinton and B. A. Auvine, 1993: Three years of rainfall over the Indian Ocean. *Bull. Amer. Meteor. Soc.*, **74**, 581-590.

Moller, C. C. and S. A. Ackerman, 1994: Application of geostationary, polar orbiting and aircraft remotely sensed radiances to a cloud catalogue. To be presented at the AMS 7th Conference on Satellite Meteorology and Oceanography

REFERENCES

Adler, RF; Negri, AJ; Keehn, PR; Hakkarinen, IM (1993): Estimation of monthly rainfall over Japan and surrounding waters from a combination of low-orbit microwave and geosynchronous IR data. *J. Appl. Meteorol.* **32**, 335 356.

Garand, L (1988): Automated recognition of oceanic cloud patterns. Part 1: Methodology and application to cloud climatology. *J. Climate* **1**, 20 39.

Goodman, B; Martin, DW; Menzel, WP; Cutrim, EC (1993): A non-linear algorithm for estimating three-hourly rain rates over Amazonia from GOES/VISSR observations. *Remote Sens. Rev.* in press.

Inoue, T (1987): An instantaneous delineation of convective rainfall areas using split window data of NOAA-7 AVHRR. *J. Meteor. Soc. Japan* **65**, 469 481.

Kummerow, C; Giglio, L (1992): A passive microwave/infra-red technique for overcoming sampling limitations of TRMM. In: Proceedings: International Workshop on the Processing and Utilization of the Rainfall Data Measured from Space. (Ed: Communication Research Laboratory) Japan Interchange of Science and Technology Center, Tokyo, 267 271.

Martin, DW; Howland, MR (1986): Grid history: A geostationary satellite technique for estimating daily rainfall in the tropics. *J. Climate Appl. Meteor.* **25**, 184 195.

Vicente, GA; Anderson, JR (1993): Combination of satellite passive microwave and infrared data for daily rainfall estimation. In: Fourth International Conference on Precipitation: Hydrological and Meteorological Aspects of Rainfall Measurement and Predictability. Iowa Institute of Hydraulic Research, Iowa City, Iowa, 99.